PHOTONIC SENSORS / Vol. 8, No. 2, 2018: 146–156

Distributed Weak Fiber Bragg Grating Vibration Sensing System Based on 3 × 3 Fiber Coupler

Wei LI[1,2] and Jian ZHANG[1*]

[1]*National Engineering Laboratory for Fiber Optic Sensing Technology, Key Laboratory of Fiber Optic Sensing Technology and Information Processing of EMC, Wuhan University of Technology, Wuhan, 430070, China*

[2]*College of Electronic and Information Engineering, Hankou University, Wuhan, 430212, China*

[*]Corresponding author: Jian ZHANG E-mail: zhangjian0716@126.com

Abstract: A novel distributed weak fiber Bragg gratings (FBGs) vibration sensing system has been designed to overcome the disadvantages of the conventional methods for optical fiber sensing networking, which are: low signal intensity in the usually adopted time-division multiplexing (TDM) technology, insufficient quantity of multiplexed FBGs in the wavelength-division multiplexing (WDM) technology, and that the mixed WDM/TDM technology measures only the physical parameters of the FBG locations but cannot perform distributed measurement over the whole optical fiber. This novel system determines vibration events in the optical fiber line according to the intensity variation of the interference signals between the adjacent weak FBG reflected signals and locates the vibration points accurately using the TDM technology. It has been proven by tests that this system performs vibration signal detection and demodulation in a way more convenient than the conventional methods for the optical fiber sensing system. It also measures over the whole optical fiber, therefore, distributed measurement is fulfilled, and the system locating accuracy is up to 20 m, capable of detecting any signals of whose drive signals lower limit voltage is 0.2 V while the frequency range is 3 Hz – 1 000 Hz. The system has the great practical significance and application value for perimeter surveillance systems.

Keywords: 3 × 3 fiber coupler; distributed fiber Bragg grating; vibration sensing system; demodulation method research

Citation: Wei LI and Jian ZHANG, "Distributed Weak Fiber Bragg Grating Vibration Sensing System Based on 3 × 3 Fiber Coupler," *Photonic Sensors*, 2018, 8(2): 146–156.

1. Introduction

As a typical representation of the wavelength-division multiplexing (WDM) technology, the fiber Bragg grating (FBG) quasi-distributed sensing technology has such advantages as high signal intensity, rapid transmission, and multi-parameter networking, however, the quantity of multiplex FBGs is only up to dozens due to the limit of the light source band width and therefore cannot meet the application requirement. A. D. Kersey *et al*. demodulated the serial signals using the Fabry-Perot filter and recognized accurately 4 different FBGs by means of the wavelength resolution method [1]. Afterwards, M. A. Davis *et al.* set three FBGs in serial in one optical fiber and performed wavelength demodulation using the Fabry-Perot filter and the

Received: 22 February 2017 / Revised: 7 January 2018

DOI: 10.1007/s13320-018-0410-3
Article type: Regular

matching gratings [2]. Then, Youlong Yu *et al.* achieved the wavelength demodulation of 10 FBGs using the WDM technology [3].

In the time-division multiplexing (TDM) technology based on the scattering effect, the sensing distance and sensitivity of the system are limited due to the weakness of the signals. K. N. Choi constructed their phase-sensitive optical time domian reflectometry (ϕ-OTDR) system in 2003, using fiber laser smaller than 3 kHz in line width, electro-optic modulator, and two-stage amplification. The system is successfully applied in the distributed fiber-optic sensing ground invasion detection system, with 1 km locating accuracy, 12 km locating range, and a signal-to-noise ratio of approximately 5.6 dB [4]. In 2005, J. C. Juarez achieved 100 m spatial resolution on 12 km sensing optical fiber using the phase sensitive OTDR technology by detecting external vibration location with narrow line width and low frequency shift laser [5]. However, the signal-to-noise ratio for the vibration location signals was poor due to the influence from the environment noise and the low Rayleigh scattering coefficient of only $10^{-7}/\mathrm{m}$ as the measurement and calculation of the location signals were done through the Rayleigh curve variation before and after the vibration. In order to improve the locating accuracy and detection sensitivity so that weak vibration signals could be detected, researchers generally adopted the moving average [6] and wavelet threshold denoising methods [7] for earlier stage noise reduction.

The mixed WDM/TDM technology could improve the problems of low signal intensity in TDM and the limited quantity of multiplexed sensors in WDM, but only the physical parameters of FBG locations can be measured, making it impossible to perform distributed measurement over the whole optical fiber. Moreover, research on the mixed WDM/TDM networking technology largely remains in the stage of theoretical simulation and analysis [8–13].

This paper describes a novel weak FBG arrays vibration sensing system based on the 3×3 fiber coupler designed that the system locates external vibration points using the TDM technology and determines perturbation behaviors in the optical fiber lines utilizing the intensity variation of the interference signals between adjacent FBG reflected signals. The reflectivity of the weak FBG is much higher than the Rayleigh back scattering coefficient in the ϕ-OTDR system, so the intensity of the FBG reflected signals is much higher than that of the Rayleigh scattering light, therefore the novel system has a higher signal-to-noise ratio and is more convenient for signal detection and demodulation. Furthermore, the novel vibration sensing system based on the 3×3 fiber coupler designed in this paper determines external perturbation through interference signals, and therefore it can perform distributed sensing and measurement, the same as the ϕ-OTDR system and also with a high spatial resolution.

2. Interference principle analysis of distributed weak fiber Bragg grating vibration sensor system

The proposed conceptual diagram of the distributed fiber Bragg grating vibration sensing system is shown in Fig. 1, and the laser is directly modulated by the field programmable gate array (FPGA). The modulated optical signal is amplified by using an erbium doped fiber amplifier (EDFA) and goes through FBG sensors via circulator. The reflected light of fiber gratings in the array reflect back to Port 3 of the circulator at a different time. Since only two light beams with equal optical path lengths will interfere, a Michelson interferometer is added to Port 3 of the circulator in the system in order to make the reflected lights of the two adjacent FBGs interfere. The length difference of the two arms of the interferometer is equal to the distance between adjacent FBGs so as to compensate the optical path difference between the two adjacent

FBGs. The optical signals reflected by the two adjacent FBGs are reflected into four light beams after entering the arms of the Michelson interferometer, of which two beams' optical path lengths are equal, so these two beams interfere in the coupler. The schematic diagram of the reflected light interference is shown in Fig. 2. The number N of gratings in the grating array produces a total of $N-1$ interference beams. The interference signal passes the photodetector and becomes a voltage signal. The FPGA generates another pulse signal at the same time, triggering the data acquisition card (DAQ card) to collect the voltage signal detected by the photodetector. The voltage signal is phase demodulated by LabVIEW software programming.

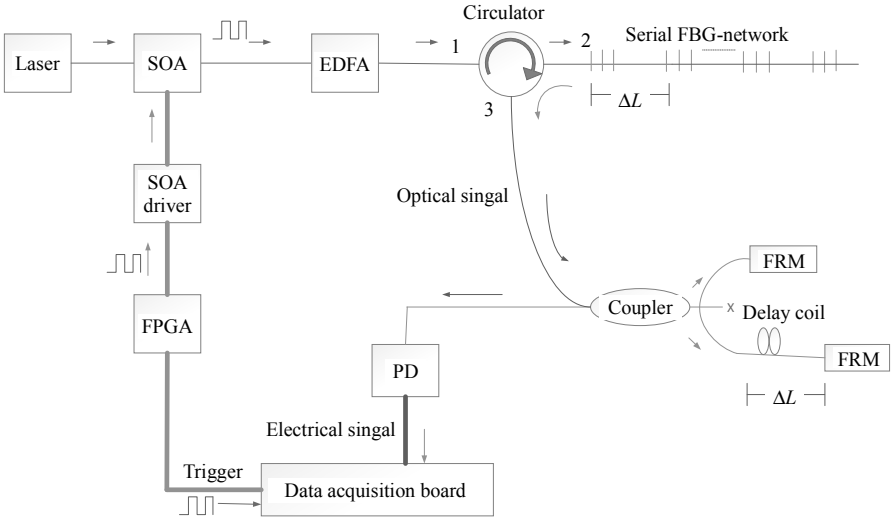

Fig. 1 Principle diagram of the distributed weak fiber Bragg grating vibration sensor system.

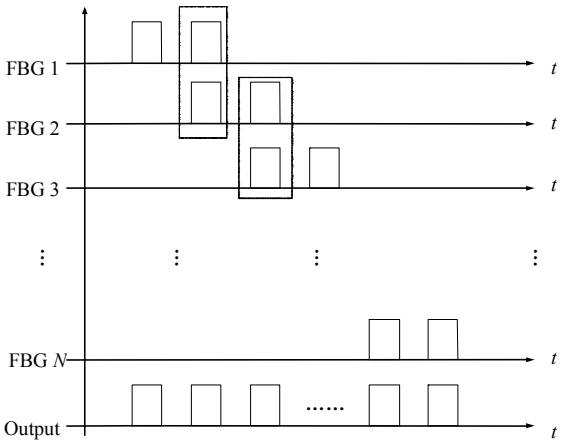

Fig. 2 Principle diagram of fiber Bragg grating array reflected light interference.

When the disturbance occurs in the fiber between two gratings, the length or refractive index of the fiber between two fiber gratings will change, which causes the change in phase and amplitude of the interference signal accordingly. However, the amplitude of the interference signal in the other sensing area (the optical fiber between adjacent gratings is a sensing area) does not change, subsequently, this feature can be used to determine the outside disturbance.

Assuming there are n gratings in the fiber grating array, the mathematical model of the reflected light incident to a 3-dB coupler light field is

$$R_{\mathrm{FBG}}=\sum_{m=1}^{n}E_0R_m\exp\mathrm{i}(\omega t+2n_{\mathrm{eff}}k_0L_m)\mathrm{rect}\left(\frac{t-\tau_m}{W}\right) \tag{1}$$

where E_0 is the amplitude of the light emitted by the laser, ω is the frequency of light (Hz), $k_0=2\pi/\lambda$ is the number of waves in vacuum (m^{-1}), L_m is the distance from the mth fiber grating to the coupler, R_m is the reflectivity of the mth fiber grating, n_{eff} is the refractive index of the optical fiber core, τ_m is the delay time of the mth fiber grating corresponding to the first grating (m), and W is the width of the light pulse (m).

When $0 \le [(t-\tau_m)/W] \le 1$, $\mathrm{rect}\left(\frac{t-\tau_m}{W}\right)=1$.

The reflected light is split into reference arm and sensing arm through the 3-dB coupler, and the two beams are shown as

$$E_{r0}=\frac{1}{\sqrt{2}}\sum_{m=1}^{n}E_0R_m\exp\mathrm{i}(\omega t+2n_{\mathrm{eff}}kL_m)\times \mathrm{rect}\left(\frac{t-\tau_m}{W}\right) \tag{2}$$

$$E_{s0}=\frac{1}{\sqrt{2}}\sum_{m=1}^{n}E_0R_m\exp\mathrm{i}(\omega t+2n_{\mathrm{eff}}kL_m)\times \mathrm{rect}\left(\frac{t-\tau_m}{W}\right) \tag{3}$$

where E_{r0} is the light field of the reflected light into the reference arm through the 3-dB coupler, and E_{s0} is the light field of the reflected light into the sensor arm through the 3-dB coupler.

After the beams are reflected by the reflective end face and returned to the 3-dB coupler, two beams are

$$E_r=\frac{1}{\sqrt{2}}\sum_{m=1}^{n}E_0R_mR_f\exp\mathrm{i}(\omega t+2n_{\mathrm{eff}}k_0L_m+2k_0n_{\mathrm{eff}}L_r)\times \mathrm{rect}\left(\frac{t-\tau_m}{W}\right) \tag{4}$$

$$E_s=\frac{1}{\sqrt{2}}\sum_{m=1}^{n}E_0R_mR_f\exp\mathrm{i}(\omega t+2n_{\mathrm{eff}}k_0L_m+2k_0n_{\mathrm{eff}}L_s)\times \mathrm{rect}\left(\frac{t-\tau_m}{W}\right) \tag{5}$$

where R_f is the reflectivity of the end face of the reflective fiber, L_r is the length of the reference arm fiber (m), and L_s is the length of the sensing arm fiber (m).

Assuming that the length of the sensing arm fiber is longer than that of the reference arm by 20 m, the optical paths of the reflected light of the *m*th grating transmitted to the end face of the sensing arm fiber and reflected back to the coupler are same with the reflected light of the reflected light of the (m + 1)th grating transmitted to the end face of reference arm fiber and reflected back to the coupler, where two reflected lights interfere at the coupler.

The two reflected lights are

$$E_{r\_m+1}=\frac{1}{\sqrt{2}}E_0R_{m+1}R_f\exp\mathrm{i}(\omega t+2n_{\mathrm{eff}}k_0L_{m+1}+2k_0n_{\mathrm{eff}}L_r)\cdot\mathrm{rect}\left(\frac{t-\tau_{m+1}}{W}\right) \tag{6}$$

$$E_{s\_m}=\frac{1}{\sqrt{2}}E_0R_mR_f\exp\mathrm{i}(\omega t+2n_{\mathrm{eff}}k_0L_m+2k_0n_{\mathrm{eff}}L_s)\times \mathrm{rect}\left(\frac{t-\tau_m}{W}\right) \tag{7}$$

where E_{r_m+1} is the light field of the reflected light of the $(m+1)$th grating into the reference arm, and E_{s_m} is the light field of the reflected light of the *m*th grating into the sensing arm.

The signals of the reference arm and sensing arm interfere at the 3-dB coupler, and the intensity of the output light is shown as follows:

$$\begin{aligned}I_{\mathrm{PD}}&=(E_{r\_m+1}+E_{s\_m})\cdot(E_{r\_m+1}+E_{s\_m})^*\\&=E_{r\_m+1}E_{r\_m+1}{}^*+E_{s\_m}E_{s\_m}{}^*\\&\quad+E_{s\_m}E_{r\_m+1}{}^*+E_{r\_m+1}E_{s\_m}{}^*.\end{aligned} \tag{8}$$

The first item and second item are the direct current (DC) components, and the third item and fourth item are the alternating current (AC) components as follows:

$$E_{s\_m}E_{r\_m+1}{}^*=\frac{1}{2}E_0{}^2R_{m+1}R_mR_f{}^2\exp\mathrm{i}[2n_{\mathrm{eff}}k_0(L_m+L_s-L_{m+1}-L_r)]\times \mathrm{rect}\left(\frac{t-\tau_{m+1}}{W}\right)\mathrm{rect}\left(\frac{t-\tau_m}{W}\right) \tag{9}$$

$$E_{s\_m}{}^*E_{r\_m+1}=\frac{1}{2}E_0{}^2R_{m+1}R_mR_f{}^2\exp\mathrm{i}[2n_{\mathrm{eff}}k_0(L_{m+1}+L_r-L_m-L_s)]\times \mathrm{rect}\left(\frac{t-\tau_{m+1}}{W}\right)\mathrm{rect}\left(\frac{t-\tau_m}{W}\right). \tag{10}$$

According to the experimental parameter settings, the two values should be zero, however, in the actual experiment, the length of the fiber can change when there are external disturbances

between two gratings, and the value of $L_m + L_s - L_{m+1} - L_r$ and $L_{m+1} + L_r - L_m - L_s$ is not zero. If $L_m + L_s - L_{m+1} - L_r = \Delta L$:

$$\begin{aligned} &2n_{\text{eff}}k_0(L_{m+1} + L_r - L_m - L_s) \\ &= -2n_{\text{eff}}k_0(L_m + L_s - L_{m+1} - L_r) \\ &= 2n_{\text{eff}}k_0\Delta L = \Delta\varphi_s + \Delta\varphi_0 \end{aligned} \tag{11}$$

where $\Delta\varphi_s$ is the phase change caused by external disturbances, $\Delta\varphi_0$ is the system inherent phase difference without any external disturbances, and the sum of the third term and the fourth term is

$$\begin{aligned} &E_{s\_m}E_{r\_m+1}^{*} + E_{s\_m}^{*}E_{r\_m+1} \\ &= \frac{1}{2}E_0^{\,2}R_{m+1}R_mR_f^{\,2}\left\{\exp\mathrm{i}[2n_{\text{eff}}k_0\Delta L] + \exp\mathrm{i}[-2n_{\text{eff}}k_0\Delta L]\right\}\times \\ &\quad \text{rect}\left(\frac{t-\tau_{m+1}}{W}\right)\text{rect}\left(\frac{t-\tau_m}{W}\right) \\ &= \frac{1}{2}E_0^{\,2}R_{m+1}R_mR_f^{\,2}\cos(2n_{\text{eff}}k_0\Delta L)\times \\ &\quad \text{rect}\left(\frac{t-\tau_{m+1}}{W}\right)\text{rect}\left(\frac{t-\tau_m}{W}\right). \end{aligned} \tag{12}$$

The signal detected by the photodetector can be represented by the following equation:

$$I_D \propto [A + \cos(\Delta\varphi_s + \Delta\varphi_0)] \tag{13}$$

when the piezo-electric transducer (PZT) is applied on the two adjacent fiber gratings and driven by a signal with fixed frequency ω, the phase change is $\Delta\varphi_s = \cos(\omega t)$, as shown in the following equation:

$$I_D \propto [A + \cos(\Delta\theta)] \propto [A + \cos(\cos\omega t + \Delta\varphi)]. \tag{14}$$

The phase in the driving signal can be demodulated by the 3 × 3 coupler demodulation scheme.

3. 3 × 3 fiber coupler demodulation structure scheme analysis

The Michelson interferometer structure model based on the 3×3 coupler diagram is shown in Fig. 3, PD is expressed as photoelectric detector, and FRM represents as faraday rotation mirror. The light beam from the light source is reflected by Faraday rotation mirrors in the reference arm and the signal arm of the Michelson interferometer when it passes the circulator and the 3×3 coupler. The reflected lights interfere at the coupler. The polarization state of the interference light beams randomly fluctuates in the interferometer. And the signal attenuation caused by the polarization can be eliminated by the Faraday rotary mirrors.

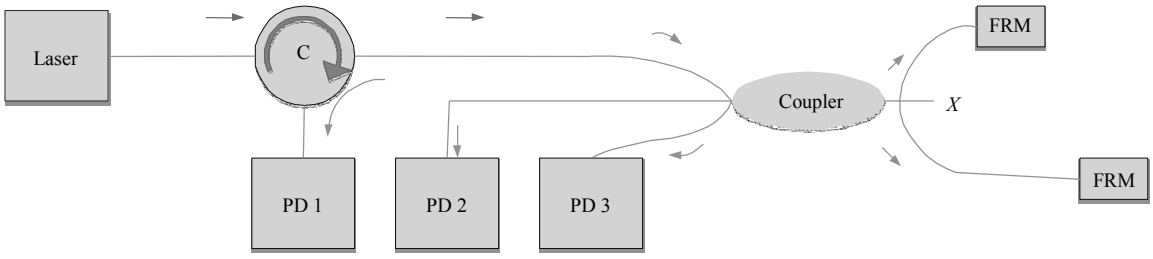

Fig. 3 Michelson interferometer structure diagram based on the 3 × 3 fiber coupler.

Taking into account the asymmetry of the actual coupler's ports, the optical path loss, and the echo, the actual output light intensity of the three ports of the interferometer is as follows:

$$I_k = D - I_0\sin\left[\varphi(t) + (k-1)\times(2\pi/3)\right],\quad k = 1,2,3 \tag{15}$$

where $\varphi(t) = \phi(t) + \psi(t)$, D is the average output light intensity, I_0 is the peak intensity of the interference fringe, k is the output optical path number, $\phi(t)$ is the phase difference signal of the sensor, i.e., the signal to be measured, and $\psi(t)$ is the phase difference caused by the changes in the actual environment. The phase difference between each other of the three signals is $2\pi/3$. 3 × 3 coupler's demodulation mathematical model is shown in Fig. 4: the gains of the adder, differentiator, multiplier, squarer, and divider corresponding to A_1 to A_7, respectively. The phase of the signal to be

measured can be obtained by the demodulation method based on the 3×3 coupler.

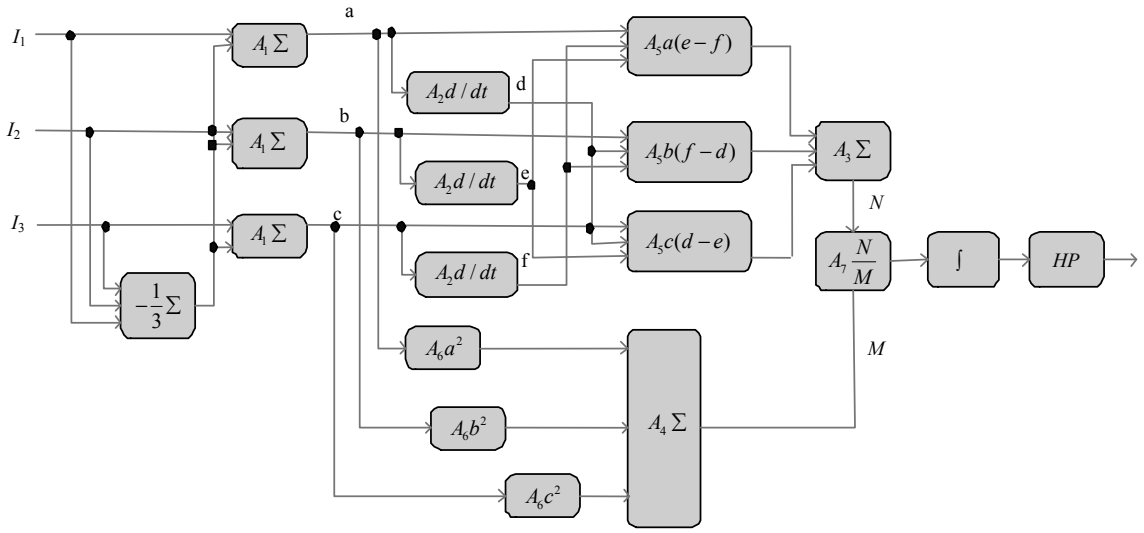

Fig. 4 Interferometer phase demodulation mathematical model based on the 3×3 fiber coupler.

4. Novel distributed weak fiber Bragg grating vibration sensor experiment system design

The experimental setup with identical weak fiber Bragg gratings (wFBGs) is shown in Fig. 5. One hundred identical wFBGs, whose length of each is less than 1 cm, are distinguished with an equal separation of 20 m using the on-line writing technique so that the total length of the identical wFBG fiber is about 2 km. The central wavelength of each identical wFBG is 1550.950 nm, and the reflectivity is about 0.08%.

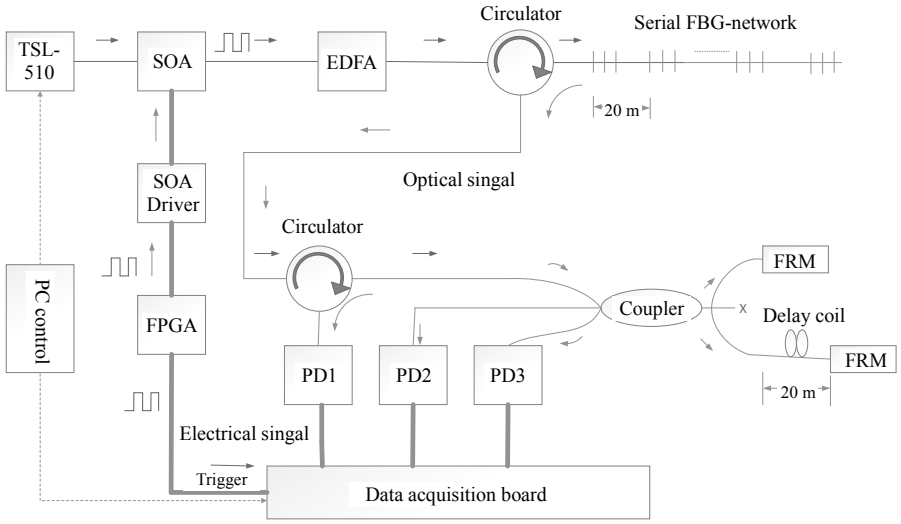

Fig. 5 Distributed weak fiber Bragg grating vibration sensing system structure diagram based on the 3×3 fiber coupler.

The light source is laser. This 1550.950-nm continuous wave light is injected into a semiconductor optical amplifier (SOA) to generate the input pulse serial, which is directly modulated by the field programmable gate array (FPGA). The width of the input pulse serial is 100 ns (which obeys the principle $cW/2n_{\text{eff}} < 20\text{m}$), and the repetition rate is fixed at 10 kHz. The time interval among the pulses should be larger than the round trip time that the pulses travel in the fiber to keep only one pulse

inside the fiber. For the 10-kHz repetition rate, the maximum fiber length is 10 km theoretically which is determined by $L \le Tc / 2n_{\text{eff}}$.

The light pluses are launched into the identical wFBG fiber by a circulator. The reflections of the wFBGs are injected into an unbalanced Michelson interferometer which consists of a circulator (C), a 3×3 coupler, and two FRMs. The final interference signals output from the 3×3 coupler are collected by three highly sensitive photodetector (PD 1 – 3), and then the signal processing scheme is accomplished by LabVIEW. In our experiment, 200 000 periods for scanning are recorded by a high-speed data acquisition board with the 100-MHz sampling rate, and the total data acquisition time is about 20 s.

The detected interference signal of one port is shown in Fig. 6. As a result of the data acquisition board set the acquisition rate as 100 M/s, the sampling points of the adjacent FBG interference signal from the rising to the falling is about 10, and the width between two interference signals is about 10 too. It also verifies the analysis in Fig. 2.

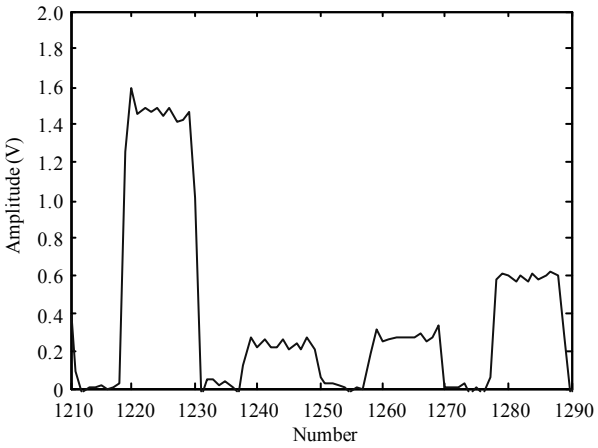

Fig. 6 Interference signal local diagram.

4.1 Parameter setting of phase demodulation experiment with distributed vibration sensing system

During this experiment, the photoelectric phase modulator made of PZT piezoelectric ceramic is used to carry out the phase modulation experiment. A part of the fiber between adjacent gratings in the grating array is wound on the PZT. The sinusoidal signal generated by the signal generator acts as the driving signal for the PZT. The frequency of the sinusoidal signal is set to 3 Hz, 5 Hz, 7 Hz, 10 Hz, 50 Hz, 100 Hz, 200 Hz, 300 Hz, 400 Hz, 500 Hz, 600 Hz, 700 Hz, 800 Hz, 900 Hz and 1000 Hz, respectively. The corresponding voltage amplitude is 0.2 V, 0.3 V, 0.4 V, 0.5 V, 1 V, 3 V, 5 V, 7 V, 9 V, and 10 V, respectively.

4.2 Processing of experimental data

4.2.1 Test of frequency response

Figure 7 shows the spectrum figure at different frequencies when the PZT driving voltage is 0.2 V. Figure 7(a) shows the spectrum of the demodulated signal at the low frequency, and Fig. 7 (b) shows the spectrum of the demodulated signal at the high frequency. As can be seen from results in the figure, the sensing system can demodulate the vibration signal when the PZT driving voltage is 0.2 V at different frequencies. When the driving voltage is 0.1 V, since the signal-noise ratio (SNR) is too small, the demodulated signal spectrum is drowned by noise and can not determine the frequency accurately.

Figure 8 is the spectrum figure of the demodulated signal processed by the fast Fourier transform when the PZT driving voltage is 5 V and the frequencies of driving sinusoidal signal are 3 Hz, 5 Hz, 7 Hz, 10 Hz, 50 Hz, 100 Hz, 200 Hz, 300 Hz, 400 Hz, 600 Hz, 700 Hz, 800 Hz, 900 Hz, and 1000 Hz, respectively. It can be seen from the figure that the frequency corresponding to the main peak of the demodulated signal is the same as the frequency of the driving sinusoidal signal, moreover, because frequency multiplication and external noise, some frequency spectra have peaks at other frequencies. Through above analysis, it can be drawn that when the driving signal voltage is not less than 0.2 V, the vibration signal from 3 Hz to 1000 Hz can be detected accurately.

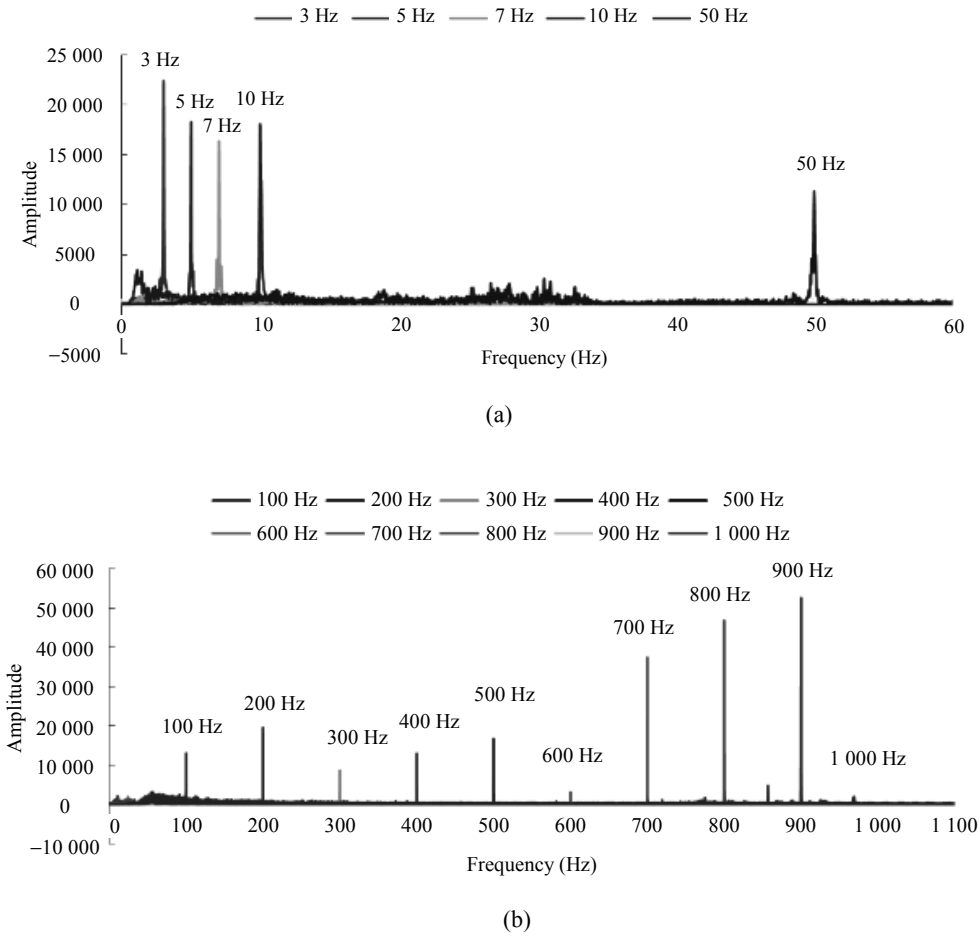

(a)

(b)

Fig. 7 Spectrum of demodulated signal at different frequencies when the sinusoidal driving voltage is 0.2 V: (a) the spectrum of the demodulated signal at the low frequencies and (b) the spectrum of the demodulated signal at the high frequencies.

4.2.2 Test of the relationship between amplitude of demodulated signal and PZT driving voltage

The phase shift of the optical wave is proportional to the radial displacement of the PZT tube, and the radial displacement of the PZT tube is proportional to the applied voltage. Therefore, the phase of the propagating light in fiber can be linearly modulated by changing voltage linearly. It can be deduced that the driving voltage of the PZT is proportional to the amplitude of the demodulated signal. In order to verify the inference, the signals collected by the sensing system under different driving voltages with frequencies of 100 Hz, 200 Hz, 300 Hz, 400 Hz, 500 Hz, and 600 Hz are demodulated. Figure 9 shows the two-dimensional graph based on the amplitude of the driving voltage and demodulated signal with the six different frequencies: the abscissa indicates the amplitude of the driving voltage with ten different frequencies: 0.2 V, 0.3 V, 0.4 V, 0.5 V, 1 V, 3 V, 5 V, 7 V, 9 V, and 10 V, respectively, and the vertical axis is the amplitude of the demodulated signal driven under ten different voltages. It can be seen from the figure that as the amplitude of the driving signal voltage increases, the amplitude of the demodulated signal increases accordingly. The PZT driving voltage is proportional to the amplitude of the demodulated signal, and the corresponding linear fits are 0.9994, 0.9958, 0.9972, 0.9894, 0.9366 and 0.9992, respectively.

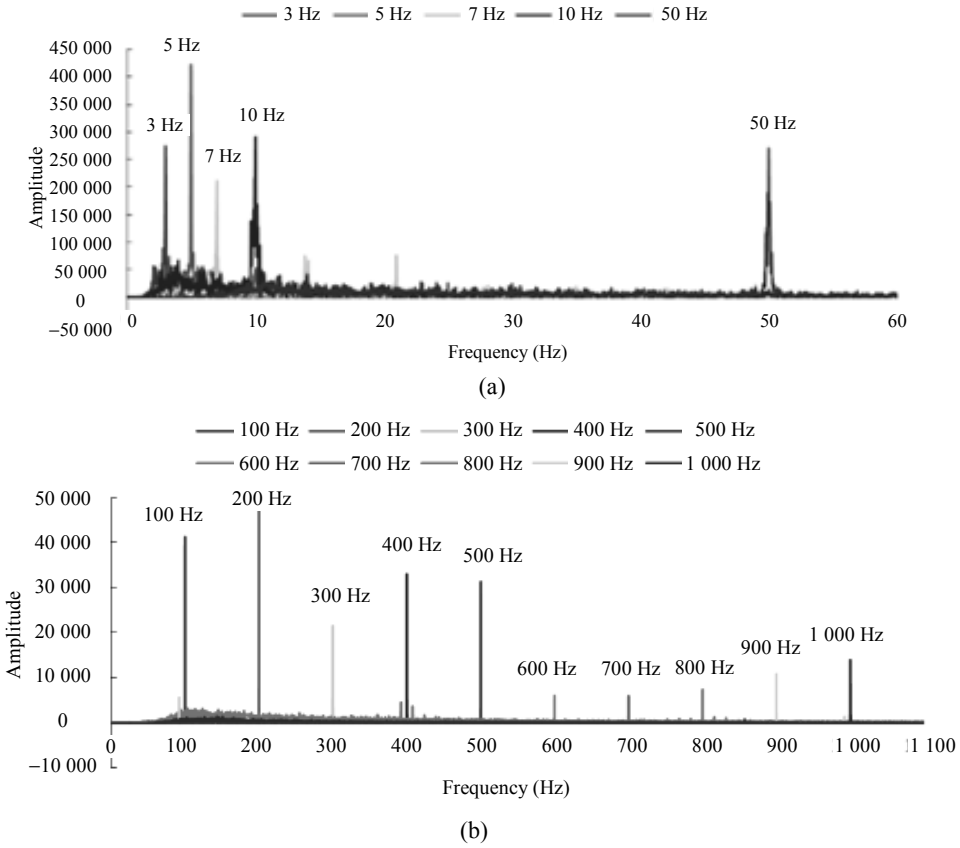

Fig. 8 Spectrum of the demodulated signal at different frequencies when the voltage of the sinusoidal driving is 5V: (a) the spectrum of demodulated signal at the low frequencies and (b) the spectrum of demodulated signal at the high frequencies.

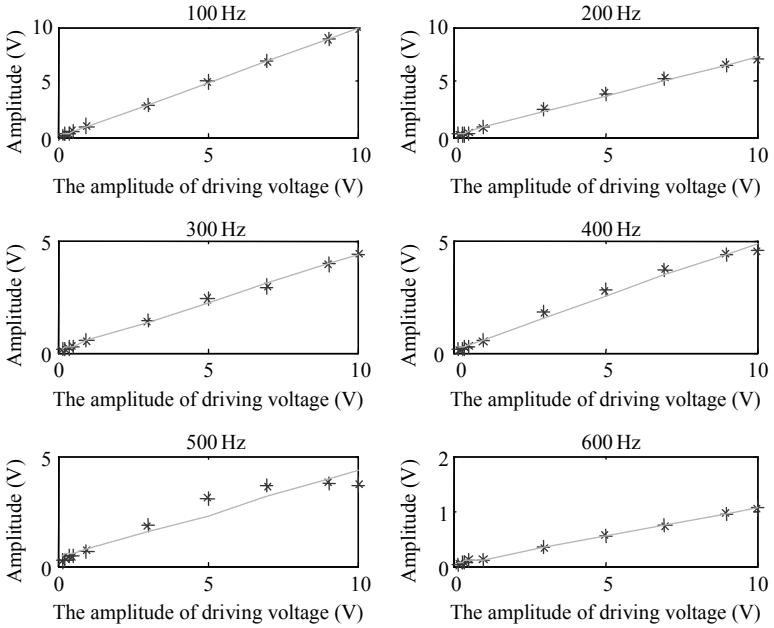

Fig. 9. Relationship between the amplitudes of the driving voltage and demodulated signal at different frequencies.

5. Conclusions

Because the signal in time-division multiplexing technology is weak and the number of fiber gratings in wavelength-division multiplexing technology is only a few dozen, the time-division and

wavelength-division multiplexing technologies can only measure the physical quantity of the location of fiber gratings without distributed measurement of the whole fiber. This paper proposes a distributed weak fiber grating vibration sensing system. The vibration system judges the vibration of the optical fiber line by the intensity change of interference signals between reflected signals of the adjacent weak fiber grating and locates the vibration points by the time-division multiplexing technique. Because the reflectivity of the weak fiber grating is much larger than the Rayleigh backscattering coefficient, the detection signal of the system is stronger than that in the vibration sensing system based on Rayleigh scattering, and it is simpler for signal detection and signal demodulation. At the same time, the vibration sensing system designed in this paper judges the external disturbance using the interference signal, so that it can carry out distributed measurement with the high spatial resolution as the vibration sensing system based on ϕ-OTDR .

In this paper, the 3 × 3 fiber coupler demodulation scheme is proposed to demodulate the phase of the detected signal, a sensing fiber area is selected in the fiber grating array, the fiber in the sensing area is wound on the PZT, and the sinusoidal signal generated by the signal generator is taken as PZT driving signal for the accuracy test of system frequency and the test of the relationship between the demodulation signal amplitude and PZT driving voltage. The result shows: when the voltage of the driving signal is not less than 0.2 V, the vibration signal with frequency between 3 Hz and 1000 Hz can be detected accurately; the amplitude of the demodulated signal is linearly related to PZT driving voltage.

Acknowledgment

This work is supported by the Major Program of the National Natural Science Foundation of China (Grant No. 61290311).

References

[1] A. D. Kersey, T. Berkoff, and W. Morey, “Multiplexed fiber Bragg grating strain-sensor system with a fiber Fabry-Perot wavelength filter,” *Optics letters*, 1993, 18(16): 1370–1372.

[2] M. A. Davis, A. D. Kersey, J. Sirkis, and E. J. Friebele, “Shape and vibration mode sensing using a fiber optic Bragg grating array,” *Smart Materials and Structures*, 1999, 5(6): 759–765.

[3] Y. L. Yu, L. F. Lui, H. Tam, and W. H. Chung, “Fiber-laser-based wavelength-division multiplexed fiber Bragg grating sensor system,” *IEEE Photonics Technology Letters*, 2001, 13(7):702–704.

[4] K. N. Choi and H. F. Taylor, “Spectrally stable Er-fiber laser for application in phase-sensitive optical time-domain reflectometry,” *Photonics Technology Letters IEEE*, 2003, 15(3): 386–389.

[5] J. C. Juarez, E. W. Maier, K. N. Choi, and H. F. Taylor, “Distributed fiber-optic Intrusion sensor system,” *Journal of Lightwave Technology*, 2005, 23(10): 2081–2087.

[6] B. Yang, W. Gao, and G. Xi, “Key technologies for based distributed fiber-optic sensing systems,” *Study on Optical Communications*, 2012, 17(2): 19–22.

[7] J. Shang and D. W. Yang, “Wavelet threshold denoising method used in disturbance sensing system,” *Modern Electronic Technology*, 2012, 35(17): 51–53.

[8] L. C. G. Valente, A. M. B. Braga, A. S Ribeiro, R. D. Regazzi, W. Ecke, C. Chojetzki, *et al.*, “Time and wavelength multiplexing of fiber Bragg grating sensors using a commercial OTDR,” in *Proceeding of Optical Fiber Sensors Conference Technical Digest, 15th IEEE Ofs*, Portland, OR, USA, 2002, pp. 01000524-1–01000524-4.

[9] W. H. Chung, H. Y. Tam, P. K. A. Wai, and A. Khandelwal, “Time- and wavelength-division multiplexing of FBG sensors using a semiconductor optical amplifier in ring cavity configuration,” *IEEE Photonics Technology Letters*, 2005, 17(12): 2709–2711.

[10] B. Dong, S. Y. He, S. Y. Hu, D. W. Tian, J. F. Lv, and Q. D. Zhao, “Time-division multiplexing fiber grating sensor with a tunable pulsed laser,” *IEEE Photonics Technology Letters*, 2006, 18(24):

2620–2622.
[11] Y. B. Dai, Y. J. Liu, J. S. Leng, G. Deng, and A. Asundi, "A novel time-division multiplexing fiber Bragg grating sensor interrogator for structural health monitoring," *Optics and Lasers in Engineering*, 2009, 47(10): 1028–1033.
[12] Y. M. Wang, J. M. Gong, D. Y. Wang, B. Dong, W. H. Bi, and A. B. Wang, "A quasi-distributed sensing network with time division multiplexing fiber Bragg gratings," *IEEE Photonics Technology Letters*, 2011, 23(2): 70–72.
[13] M. Zhang, Q. Sun, Z. Wang, X. Li, and H. Liu, "A large capacity sensing network with identical weak fiber Bragg gratings multiplexing," *Optics Communications*, 2012, 285(13): 3082–3087.